Journal of Materials Chemistry B

RSC Publishing

PAPER

View Article Online
View Journal | View Issue

Cite this: J. Mater. Chem. B, 2013, 1, 4135

Polythiophene-*g*-poly(ethylene glycol) graft copolymers for electroactive scaffolds

Anca-Dana Bendrea,†[ab] Georgina Fabregat,†[bc] Juan Torras,[d] Silvana Maione,[bc] Luminita Cianga,[a] Luis J. del Valle,[b] Ioan Cianga*[a] and Carlos Alemán*[bc]

Received 14th May 2013
Accepted 17th June 2013

DOI: 10.1039/c3tb20679c

www.rsc.org/MaterialsB

The properties, microscopic organization and behavior as the cellular matrix of an all-conjugated polythiophene backbone (PTh) and well-defined poly(ethylene glycol) (PEG) grafted chains have been investigated using different experimental techniques and molecular dynamic simulations. UV-vis spectroscopy has been used to determine the optical band gap, which has been found to vary between 2.25 and 2.9 eV depending on the length of the PEG chains and the chemical nature of the dopant anion, and to detect polaron → bipolaron transitions between band gap states. The two graft copolymers have been found to be excellent cellular matrices, their behavior being remarkably better than that found for other biocompatible polythiophene derivatives [*e.g.* poly(3,4-ethylenedioxythiophene)]. This is fully consistent with the hydrophilicity of the copolymers, which increases with the molecular weight of the PEG chains, and the molecular organization predicted by atomistic molecular dynamics simulations. Graft copolymers tethered to the surface tend to form biphasic structures in solvated environments (*i.e.* extended PTh and PEG fragments are perpendicular and parallel to the surface, respectively) while they collapse onto the surface in desolvated environments. Furthermore, the electrochemical activity and the maximum of current density are remarkably higher for samples coated with cells than for uncoated samples, suggesting multiple biotechnological applications in which the transmission with cells is carried out at the electrochemical level.

Introduction

The discovery of a new class of organic polymers with conducting properties in the late 1970s opened up a new era in the field of polymer science.[1] In the last few decades conducting polymers (CPs) have attracted considerable interest because of their interesting electrical, electrochemical, optical and magnetic properties.[2] Among them, polyheterocycles such as polypyrrole (PPy), polythiophene (PTh), polyaniline (PAni) and some of their derivatives have received particular attention because they exhibit good stabilities, good conductivities and ease of synthesis.[2–4] PTh derivatives have been settled among the most promising CPs for technological applications, poly(3-hexylthiophene) and, especially, poly(3,4-ethylenedioxythiophene) (PEDOT) being the most popular. PEDOT (Scheme 1), which exhibits low band gap (1.6–1.7 eV), high conductivity (up to 550 S cm^{-1}) and good environmental stability,[5–7] has been employed to fabricate electrochromic devices,[8] fuel cells,[9] field emitters[10] and dye-sensitized solar cells (DSSCs).[11]

Most CPs present a number of important advantages for biomedical applications, including biocompatibility, ability to entrap and controllably release biological molecules (*i.e.* reversible doping), ability to transfer charge from a biochemical reaction, and the potential to easily alter the electrical, chemical, physical, and other properties of the CPs to better suit the nature of the specific application. These unique characteristics are useful in many biomedical applications, such as biosensors, tissue-engineering scaffolds, neural probes, drug-delivery devices, and bio-actuators. Biomedical applications of CPs have been recently reviewed.[12,13] In spite of this, there is always a desire to further optimize a material for a specific application. The two common properties desired for all biomedical

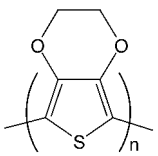

Scheme 1 Chemical structure of PEDOT.

[a]"Petru Poni" Institute of Macromolecular Chemistry, 41A, Grigore–Ghica Voda Alley, 700487, Iasi, Romania. E-mail: ioanc@icmpp.ro

[b]Departament d'Enginyeria Química, E. T. S. d'Enginyers Industrials, Universitat Politècnica de Catalunya, Diagonal 647, 08028 Barcelona, Spain. E-mail: carlos.aleman@upc.edu

[c]Center for Research in Nano-Engineering, Universitat Politècnica de Catalunya, Campus Sud, Edifici C', C/Pasqual i Vila s/n, Barcelona E-08028, Spain

[d]Department of Chemical Engineering, Igualada School of Engineering, Universitat Politècnica de Catalunya, Pça Rei 15, Igualada 08700, Spain

† These authors contributed equally to this work.

applications are biocompatibility and redox stability (*i.e.* electroactivity and electrochemical stability), but beyond these needs, CP modifications tend to be specific for the application. For example, it is important to improve the ability of CPs to act as a bioactive platform for cellular proliferation. This can be achieved physically (*i.e.* physical adsorption of molecules that enhance proliferation of a variety of cell types) or chemically (*i.e.* functionalizing the CPs with the desired molecules through chemical bonds). Functionalization of CPs with different molecules has allowed biomedical engineers to modify CPs with biological sensing elements, and to turn on and off different signaling pathways to create CPs that enhance cellular adhesion and proliferation and improve their biocompatibility.[14–17]

Among polymer–polymer hybrid materials, graft copolymers made of components with very different properties are receiving increasing attention.[18–23] Graft copolymers amplify the characteristic properties of their individual components, exhibiting unusual features because of their confined structure, compact organization and notable chain end effects. Within this context, copolymers formed by an all conjugated polythiophene (PTh) backbone and other polymeric grafted chains have been prepared to improve the very limited processability and solubility of unsubstituted PTh [*e.g.* poly(methyl acrylate)[24,25] and polystyrene[26,27]], to fabricate donor–π–acceptor molecular species [*e.g.* poly(styrene-*graft*-C_{60})[28]] or to prepare hydrophilic conducting surfaces [*e.g.* poly(ethylene glycol) monomethacrylate[29]].

In a very recent study, we reported the synthesis and characterization of hybrid materials made of well-defined poly(ethylene glycol) (PEG) chains grafted to the conducting PTh backbone, which were denoted as PTh-*g*-PEG_n (where n refers to the molecular weight of PEG chains).[30] PEG is a biocompatible hydrophilic polymer with many practical applications in biology, biotechnology and biomedicine,[31,32] which is frequently used for the fabrication of polymer–biomolecule,[33,34] polymer–polymer[35] and polymer–inorganic[36,37] hybrid materials. The fabrication of PTh-*g*-PEG_n (Scheme 2) was achieved through a two-step process, which consisted of the chemical synthesis of macromonomers (*i.e.* pentathiophene substituted with PEG chains of $M_w = 1000$ or 2000) and the anodic polymerization of such macromonomers.[30] The chemical structure, composition, morphology and electrochemical properties of the resulting materials, PTh-*g*-PEG_{1000} and PTh-*g*-PEG_{2000}, were investigated using FTIR, X-ray photoelectron spectroscopy (XPS), scanning electron microscopy (SEM), atomic force microscopy (AFM) and cyclic voltammetry (CV). Furthermore, the ability of these hybrids to adsorb both extracellular and plasma proteins was investigated, their affinity towards globular proteins being higher than towards fibrillar proteins.[30]

This work is mainly focused on the electronic, electrochromic and superficial properties, internal organization at the molecular level and behavior as the cellular matrix of PTh-*g*-PEG_{1000} and PTh-*g*-PEG_{2000}. More specifically, the electronic and electrochromic properties of the hybrids have been investigated using UV-vis spectroscopy. After this the surface wettability of the graft copolymers has been examined and compared with that of poly(3,4-ethylenedioxythiophene) (PEDOT), a polar PTh derivative that was proved to enhance cellular adhesion and proliferation,[38,39] by measuring the contact angle. Next, the relative organization of the PTh backbone and the PEG side chains in graft copolymers has been examined using atomistic Molecular Dynamics (MD) simulations. For this purpose, an assembly formed by two copolymer molecules deposited in a surface has been simulated considering both desolvated (*i.e.* gas-phase) and aqueous solution environments. Finally, the biocompatibility and behavior of the two hybrids as biological platforms have been examined using cellular adhesion and proliferation assays. The latter issue is particularly relevant since the results have allowed us to demonstrate that chemical modification of PTh chains by grafting biocompatible PEG results in a material with enhanced properties as bioactive platforms.

Methods

Synthesis

The macromonomers used for the anodic polymerization of PTh-*g*-PEG_{1000} and PTh-*g*-PEG_{2000} consisted of pentathiophene bearing a PEG chain of $M_w = 1000$ and $M_w = 2000$, respectively, at the central thiophene ring. These macromonomers, hereafter denoted as Th_5-PEG_{1000} and Th_5-PEG_{2000} (Scheme 3), were prepared by chemical synthesis using the route described in ref. 30.

On the other hand, PTh-*g*-PEG_n graft copolymers were prepared by chronoamperometry (CA) under a constant potential using an Autolab PGSTAT302N equipped with the ECD module (Ecochimie, The Netherlands). All polymerizations were carried out in a standard three-electrode cell under nitrogen atmosphere (99.995% in purity) at room temperature. The

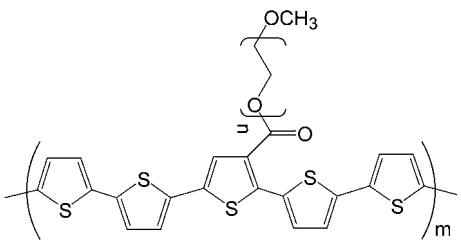

PTh-*g*-PEG_{1000}: n = 22

PTh-*g*-PEG_{2000}: n = 44

Scheme 2 Chemical structure of PTh-*g*-PEG_n.

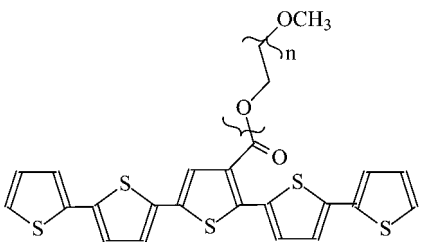

Th_5-PEG_{1000}: n = 22
Th_5-PEG_{2000}: n = 44

Scheme 3

anodic compartment was filled with 15 mL of a 1×10^{-3} M Th_5-PEG_n solution in a mixture of acetonitrile : dichloromethane (50 : 50 v/v) containing 0.1 M of a supporting electrolyte, while the cathodic compartment was filled with 10 mL of the same electrolyte solution. Steel AISI 316 and indium-tin oxide (ITO) sheets of 1.0×0.5 and 0.5×0.5 cm^2, respectively, were employed as working electrodes. The counter electrode was a platinum sheet of 1.0×0.50 cm^2 while the reference electrode was an Ag/AgCl electrode containing a KCl saturated aqueous solution ($E^o = 0.222$ V at 25 °C), which was connected to the working compartment through a salt bridge containing the electrolyte solution. Graft copolymers were prepared considering the following experimental conditions:

• PTh-*g*-PEG_{1000} and PTh-*g*-PEG_{2000}: $LiClO_4$ as supporting electrolytes and a constant potential of 0.70 and 75 V, respectively.

• PTh-*g*-PEG_{2000}: Bu_4NPF_6 as the supporting electrolyte and a potential of 0.80 V.

UV-vis spectroscopy

UV-vis absorption spectra of macromonomers in solution were registered using a Specord 200 spectrophotometer. Spectra of macromonomers and PTh-*g*-PEG_n films were obtained using a UV-vis-NIR Shimadzu 3600 spectrophotometer equipped with a tungsten halogen visible source, a deuterium arc UV source, a photomultiplier tube UV-vis detector, and an InGaAs photodiode and cooled PbS photocell NIR detectors. Spectra were recorded in the absorbance mode using the integrating sphere accessory (model ISR-3100), the wavelength range being 185–3300 nm. The interior of the integrating sphere was coated with a highly diffuse $BaSO_4$ reflectance standard. Uncoated ITO glass was used as reference. Hybrid material films were deposited on ITO-glass electrodes for measurements. Single-scan spectra were recorded at a scan speed of 60 nm min^{-1}. Measurements, data collection and data evaluation were controlled by the computer software UVProbe version 2.31.

Wettability

Contact angle measurements were performed using the sessile drop method, at room temperature and controlled humidity. Images of 1 μL distilled water drops were recorded after stabilization (30 s) using a CAM-200 equipment from KSV-Finland. Contact angle values were obtained as the average of five independent measures for each sample.

Optical profilometry

The thickness of the films was determined using a WYKO 9300NT optical profiler (Veeco, Plainview, NY). Different scratches were intentionally provoked on PTh-*g*-PEG_{1000} and PTh-*g*-PEG_{2000} films and measured to allow statistical analysis of data. Imaging of the films was conducted using the following optimized settings: vertical scanning interferometry (VSI) mode, full resolution, 5 mm back scan and 10 mm primary scan, 10× and 50× Michelson LR objective lens (fields of view of 2.0×) for image sizes of 237×315 μm^2 and 64×48 μm^2, respectively.

Atomic force microscopy (AFM)

Topographic AFM images were obtained with a Molecular Imaging PicoSPM using a NanoScope IV controller under ambient conditions. The tapping mode AFM was operated at constant deflection. The row scanning frequency was set to 1 Hz and the physical tip-sample motion speed was 10 μm s^{-1}. The root-mean-square (RMS) roughness was determined using the statistical application of the Nanoscope software, which calculates the average considering all the values recorded in the topographic image with exception of the maximum and the minimum. AFM measurements were performed on various parts of the films, which produced reproducible images similar to those displayed in this work. The scan window sizes used in this work were 5×5 μm^2.

Molecular dynamics simulations

Graft copolymers were simulated using an assembly of two molecules, each one containing a backbone with 20 thiophene rings and four grafted PEG chains with 22 repeating units (Scheme 1). Accordingly, the molecular weight of the PEG chain in these model graft copolymers corresponds to that of PTh-*g*-PEG_{1000}. The two molecules were attached to the center of a square surface ($L = 133.98$ Å) formed by 900 spherical particles (*i.e.* 30×30 particles with a distance of 4.62 Å between neighboring particles) through a bond between the α-carbon of the first backbone thiophene ring and one spherical particle of the surface. The distance between the spherical particles used to attach the molecules was 26.1 Å. MD simulations were performed on two model systems, which can be described as follows:

(i) The two molecules tethered to the surface in the gas-phase. This solvent-free model corresponds to the situation encountered in AFM experiments. MD simulations of this model system involved 2462 explicit particles.

(ii) The two molecules attached to the surface in the aqueous solution. For this purpose, a spherical water cap with a radius of 70 Å and centered in the middle of tethered molecules was constructed and, subsequently, filled with 92 513 explicit water molecules. This solvated model represents the situation found in cell attachment assays. The model involved a total of 280 001 explicit particles.

The potential energy of the simulated systems was computed using the AMBER force field.[40] All the bonding and van der Waals parameters, with exception of the S–C–C–S torsion, were taken from the Generalized AMBER Force-Field (GAFF).[41] The parameters for the S–C–C–S torsion were extracted from a recent study in which force-field parameters compatible with AMBER were developed by computing the potential of mean forces for the inter-ring rotation of different 2,2′-bithiophene derivatives.[42] Atomic charges were adjusted using the Restrained ElectroStatic Potential (RESP) strategy.[43] The van der Waals parameters of the spherical particles used to construct the surface [$R = 2.35$ Å and $\varepsilon = 0.90$ kcal mol^{-1}] were extrapolated from previous studies devoted to investigate the structure of organic systems tethered to rigid surfaces.[44,45] Water molecules were represented using the TIP3P model.[46]

MD simulations were performed using the AMBER 12.0 program.[47] Simulations in aqueous solution were performed by applying an atom-pair distance cut-off at 12 Å to compute van der Waals and electrostatic interactions, whereas gas-phase simulations were performed without cut-off. Bond lengths involving hydrogen atoms were constrained using the SHAKE algorithm with a numerical integration step of 2 fs.[48] The positions of the spherical particles at the surface were restrained applying a force constant of 40 kcal mol^{-1} $Å^{-2}$.

Before starting the MD run series, 5×10^3 steps of energy minimization were performed to relax conformational and structural tensions. After this, the systems in the gas-phase and in solution were progressively heated from 0 to 298 K along 45 ps of MD and, subsequently, equilibrated at the latter temperature for 15 ps. The last snapshot of the equilibration was used as the starting point for the production series. Coordinates were saved every 10 ps for further analysis for simulation lengths of 5 ns.

Cellular adhesion and proliferation

Vero cells (African green monkey kidney epithelial cell line) were cultured in Dulbecco's modified Eagle medium (DMEM) supplemented with 10% fetal bovine serum, 1% penicillin/streptomycin and 2 mM L-glutamine at 37 °C in a humidified atmosphere of 5% CO_2 in air. The cultured medium was changed every two days and, for sub-culture, cell monolayers were rinsed with phosphate buffered saline (PBS) and detached by incubation with 0.25% trysin/EDTA for 5 min at 37 °C. Cell concentration was determined by counting at the Neubauer camera using 4% trypan blue as the vital dye. The detached cells with a viability of ≥95% were used for cultures following the conditions for the adhesion and proliferation assays.

PTh-*g*-PEG_{1000} and PTh-*g*-PEG_{2000} films deposited onto steel AISI 316 sheets of 1 cm^2 were placed in plates of 24 wells and sterilized using UV irradiation for 15 min in a laminar flux cabinet. Samples were incubated with 1 mL of culture medium for 30 min under culture conditions to equilibrate the material. Finally, the medium was aspired and the material was evaluated for cell adhesion and proliferation by exposing cells to direct contact with the material surface. An aliquot of 50 mL containing 5×10^4 cells (adhesion assays) or 2×10^4 cells (proliferation assays) was deposited on the substrate of each well. The plate was incubated under culture conditions for 60 min to promote the cell attachment to the film surface. Finally, 1 mL of the culture medium was added to each well. Controls of adhesion and proliferation were simultaneously performed by culturing cells on the surface of the tissue culture polystyrene (TCPS) plates and uncoated steel. Cell adhesion and proliferation were evaluated after 24 hours and 7 days of culture, respectively, using the MTT [3-(4,5-dimethylthiazol-2-yl)-2,5-diphenyltetrazolium bromide] assay, which determines the cell viability. The viability results were normalized to TCPS control as relative percentages.

Results were derived from the average of four replicates ($n = 4$) for each independent experiment. ANOVA and Turkey tests were performed to determine the statistical significance, which was considered at a confidence level of 95% ($p < 0.05$).

The cells on PTh-*g*-PEG_{1000} and PTh-*g*-PEG_{2000} films were examined by epifluorescence microscopy (BA410 Model, Motic Spain S.L.). For this purpose, Vero cells were fixed and permeabilized with cold acetic acid : methanol (1 : 3) for 3 min and subsequently replaced with fresh fixative for further 3 min. After draining the fixative, the air-dried material was immersed in 2 mL of stain (0.1 μg mL^{-1} bisbenzimide Hoechst 33258 in PBS) and incubated for 5 min at room temperature in the dark to stain nuclei. Then, the stain was removed and films were mounted in a nonfluorescent medium. The bisbenzimide fluorescence and intrinsic fluorescence of films were observed with standard fluorescence filter sets: a MF31000 filter (Exciter D350/50x and Emitter D460/50m) and a MF31001 filter (Exciter D480/30x and Emitter D535/40m), respectively.

Scanning electron microscopy (SEM)

SEM studies were performed using a Focussed Ion Beam Zeiss Neon 40 scanning electron microscope operating at 5 kV, equipped with an EDX spectroscopy system. Samples were mounted on a double-side adhesive carbon disc and sputter-coated with a thin layer of carbon to prevent sample charging problems. Before the carbon coating for examination, samples covered with cells were fixed in a 2.5% glutaraldehyde PBS solution overnight at 4 °C. Then, they were dehydrated by washing in an alcohol battery (30°, 50°, 70°, 90°, 95° and 100°) at 4 °C for 30 minutes per wash. Finally, samples were air-dried, and sputter-coated with carbon before SEM observation.

Electrochemical characterization

The electrochemical behavior of PTh-*g*-PEG_{1000} and PTh-*g*-PEG_{2000} was studied by cyclic voltammetry (CV) considering two different environments: films directly obtained from electropolymerization (*i.e.* as prepared samples) and films covered will cells. For this purpose, a sterilized phosphate buffer saline solution (PBS; pH = 7.2) was used as the electrolyte in the three-electrode cell. Steel sheets of 1 cm^2 area were used as counter and working electrodes, an Ag/AgCl electrode being used as the reference electrode. Cyclic voltammograms were registered at a scan rate of 50 mV s^{-1} in the potential range from −0.30 to +0.90 V. All CV assays were performed with an Autolab PGSTAT302N equipped with the ECD module (Ecochimie, The Netherlands).

The electroactivity refers to the charge storage ability and was determined by measuring the cathodic and anodic areas in the first control voltammogram (*i.e.* the electroactivity increases with the similarity between such areas). The electrochemical stability (electrostability) was evaluated by determining the loss of electroactivity with the number of consecutive oxidation–reduction cycles (LEA, in %):

$$\mathrm{LEA} = \frac{\Delta Q}{Q_{\mathrm{I}}} \times 100 \quad (1)$$

where ΔQ is the difference between the voltammetric charges (in C) of the first and the last oxidation–reduction cycle, and Q_{I} is the voltammetric charge corresponding to the first cycle. In this work all LEA values are referred to a total of 10 consecutive oxidation–reduction cycles.

Results and discussion

Electronic properties

Diluted dichloromethane solutions of Th_5-PEG_{1000} and Th_5-PEG_{2000} macromonomers (*i.e.* 0.09 and 0.18% w/w, respectively) show an absorbance peak in the UV-vis range at $\lambda_{max} = 402$ and 376 nm (Fig. 1a), respectively, which corresponds to the π–π* transition of the thiophene rings. The UV-vis spectra of Th_5-PEG_{1000} and Th_5-PEG_{2000} films, which were prepared by drop casting 20 μL of a 1 mM macromonomer solution in acetonitrile/dichloromethane (50/50) onto an ITO plate, are included in Fig. 1a. As it can be seen, the π–π* transition of Th_5-PEG_{1000} ($\lambda_{max} = 377$ nm) and Th_5-PEG_{2000} ($\lambda_{max} = 385$ nm) shows blue and red shifts, respectively, with respect to the spectra recorded for dilute solutions. Thus, the conjugation of the pentathiophene fragment in films, which relies upon overlap of the π-orbitals of the coplanar Th rings, is lower and higher than in diluted solutions for Th_5-PEG_{1000} and Th_5-PEG_{2000}, respectively. This feature evidences that grafted PEG chains play a predominant role in the electronic properties of macromonomers, their importance being expected to decrease upon polymerization.

Fig. 1b compares the UV-vis spectra of PTh-*g*-PEG_{1000} prepared using $LiClO_4$ as the supporting electrolyte with those of PTh-*g*-PEG_{2000} obtained in the presence of $LiClO_4$ and Bu_4NPF_6. The shape of three spectra are rather similar and show a broad band with λ_{max} at 400 (PTh-*g*-PEG_{1000} with $LiClO_4$), 413 (PTh-*g*-PEG_{2000} with $LiClO_4$) and 423 nm (PTh-*g*-PEG_{2000} with Bu_4NPF_6), which corresponds to the π–π* transition. The red shift with respect to the macromonomers originates from the increment of the conjugation length produced in the backbone upon polymerization. However, the width of the band reflects the coexistence of long and short effective conjugation lengths. Moreover, both PTh-*g*-PEG_{1000} and PTh-*g*-PEG_{2000} are less conjugated than poly[3-(3,6-dioxaheptyl)thiophene], an early reported PTh derivative containing small oligo(oxyethylene) substituents [*i.e.* R = –$(CH_2CH_2O)_2$–CH_3], which showed λ_{max} = 435 and 445 nm when produced by chemical and electrochemical polymerization, respectively.[49] Indeed, all these systems show less conjugation than unsubstituted PTh chemically[50] and electrochemically[51] produced (*i.e.* λ_{max} = 495 and 447 nm, respectively).

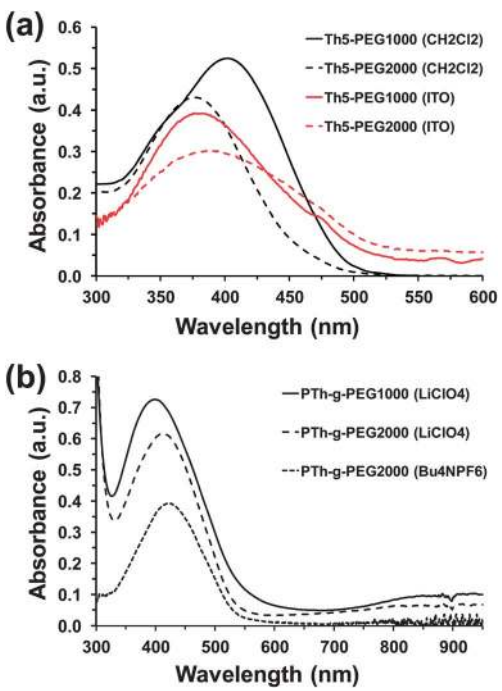

Fig. 1 UV-vis spectra of: (a) Th_5-PEG_{1000} and Th_5-PEG_{2000} macromonomers in a diluted dichloromethane solution and deposited as a film onto an ITO substrate; and (b) PTh-*g*-PEG_{1000} prepared using $LiClO_4$ as the supporting electrolyte and PTh-*g*-PEG_{2000} obtained in the presence of $LiClO_4$ and Bu_4NPF_6.

In a π-conjugated system, the band gap (ε_g) is defined as the difference between the lowest energy in the conduction band and the highest energy in the valence band. According to the zero order approximation, this is equal to the lowest excitation energy, which can be obtained from the onset value (λ^{onset}) at the lower energy edge of the absorption spectrum (*i.e.* $\varepsilon_g = 1240/\lambda^{onset}$). Specifically, the optical ε_g derived from the UV-vis spectra of PTh-*g*-PEG_{1000} ($\lambda^{onset} = 552$ nm) and PTh-*g*-PEG_{2000} ($\lambda^{onset} = 542$ nm) prepared using ClO_4^- as a dopant is 2.25 and 2.29 eV, respectively, while that obtained for PTh-*g*-PEG_{2000} doped with PF_6^- ($\lambda^{onset} = 547$ nm) is 2.27 eV. According to these values, the energy gap associated with the lowest π–π* transition of PTh-*g*-PEG_n graft copolymers is slightly larger than those of conventional PTh derivatives substituted at the 3-position [*e.g.* poly(thiophene-3-methyl acetate), 1.98–2.17 eV,[52] poly(3-chlorothiophene), 2.14 eV,[53] and poly(3-bromothiophene), 1.93–1.97 eV (ref. 54)]. This feature corroborates that the conjugation length at the backbone is lower for these graft copolymers than for derivatives with conventional substituents. Moreover, all these values are higher than the ε_g determined for PEDOT using electrochemical (1.98 eV)[55] or spectroscopic (1.6–1.7 eV)[5] methods (see Table 1), which is consistent with the excellent electrochemical and electrical behavior of this PTh derivative.

Another interesting feature is that the oxidation band observed at ~900 nm for both PTh-*g*-PEG_{1000} and PTh-*g*-PEG_{2000} when prepared in the presence of $LiClO_4$ is not detected when the supporting electrolyte is Bu_4NPF_6. This band, which can be attributed to the formation of polarons and bipolarons in PTh

Table 1 Comparison of the properties determined for PTh-*g*-PEG_{1000}, PTh-*g*-PEG_{2000} and PEDOT

	PTh-*g*-PEG_{1000}	PTh-*g*-PEG_{2000}	PEDOT
ε_g (eV)	2.25[a]	2.29[a]	1.6–1.7;[a,b] 1.98[c]
Contact angle (°)	87	76	82
Roughness (nm)	11 ± 2	12 ± 2	111 ± 19
Adhesion of Vero cells (%/cm^2)	98.7 ± 4.7[d]	101.3 ± 4.7[d]	117.3 ± 9.1[d,e]
Proliferation of Vero cells (%/cm^2)	149.2 ± 9.7[d]	166.4 ± 17.3[d]	100.0 ± 3.7[d,e]
Electroactivity (%)	162[f]	329[f]	131[e,f]

[a] Band gap determined by UV-vis spectroscopy. [b] Taken from ref. 5. [c] Band gap determined electrochemically in ref. 55. [d] The relative viability of Vero cells was established in relation to the tissue culture polystyrene (TCPS) control (*i.e.* viability of TCPS = 100%). [e] Data taken from ref. 16. [f] Enhancement of the electroactivity in films covered with cells with respect to the uncovered ones.

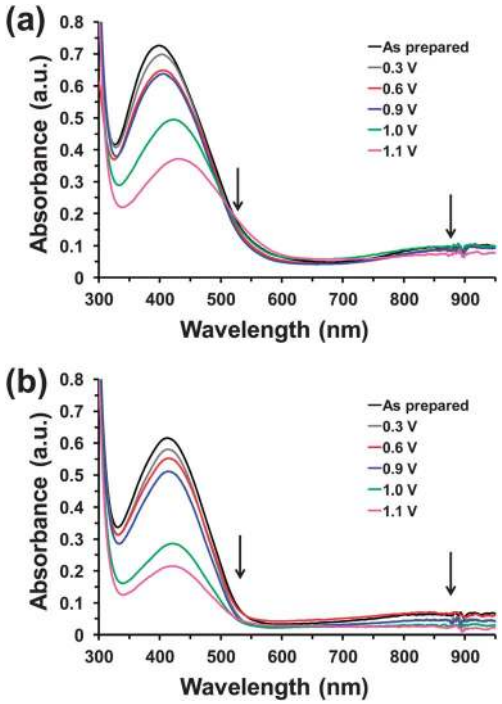

Fig. 2 UV-vis spectra of (a) PTh-*g*-PEG_{1000} and (b) PTh-*g*-PEG_{2000} doped with ClO_4^- using as-prepared samples and after re-oxidation with potentials of 0.3, 0.6, 0.9, 1.0 and 1.1 V.

chains,[52] evidences the influence of the dopant agent. Thus, the two graft copolymers form complexes with the ClO_4^- dopant anions while the vanishing of the band confirms the lack of complexes with PF_6^-.

Fig. 2 shows the effects of additional oxidation on the electronic properties of PTh-*g*-PEG_{1000} and PTh-*g*-PEG_{2000} doped with ClO_4^-. For this purpose, after the introduction of the graft copolymer films in acetonitrile solutions with 0.1 M $LiClO_4$, a constant potential was applied for 10 s. UV-vis spectra were recorded after re-oxidation with potentials of 0.3, 0.6, 0.9, 1.0 and 1.1 V. As it can be seen, this oxidation process is accompanied by the reduction and the red shift of the absorbance band that is associated with the π–π^* transition. Thus, the λ_{max} of the as-prepared PTh-*g*-PEG_{1000} and PTh-*g*-PEG_{2000} films increases from 400 and 413 nm, respectively, to 431 and 422 nm after applying a constant potential of 1.1 V for 10 s. Both the red shift and the decrease of the absorbance provoked by further oxidation are consistent with a reduction of the ε_g, which is slightly more pronounced for PTh-*g*-PEG_{1000} than for PTh-*g*-PEG_{2000}. On the other hand, the second band, which is observed at ~900 nm in the as-prepared samples, shifts into the NIR region after additional oxidation. According to previous studies, this variation, which is similar for the two graft copolymers, has been attributed to polaron → bipolaron transitions between band gap states.[56]

Regarding the electrochromic properties of graft copolymers, the as-prepared PTh-*g*-PEG_{1000} and PTh-*g*-PEG_{2000} films doped with ClO_4^- showed a brownish orange and intense yellow color, respectively, while the latter hybrid obtained using Bu_4NPF_6 as the supporting electrolyte displayed an intermediate color. Re-oxidation with potentials lower than 1.0 V does not provoke any variation in the color while films change to green and bluish green when the applied potential is 1.0 and 1.1 V, respectively. This behavior is fully consistent with that observed for conventional PThs.[57]

Surface wettability

The average values of the contact angle (θ) determined for PTh-*g*-PEG_{1000} and PTh-*g*-PEG_{2000} films doped with ClO_4^- are $\theta = 87°$ and 76°, respectively, indicating that, as expected, the enlargement of the PEG chains increases the hydrophilicity at the surface. Zhang *et al.* reported that the contact angle of unsubstituted PTh obtained by electropolymerization is higher than 100°.[58] Moreover, the same authors showed that the water-repellency of PTh increases with the thickness,[58] which was attributed to the effect of the superficial morphology on the roughness. Thus, ultrathin films are compact and smooth while the surface becomes more irregular and porous as the thickness increases, enhancing the roughness. However, the influence of the molecular weight of grafted chains on both the thickness and roughness of PTh-*g*-PEG_n has been found to be very small. Specifically, the AFM 2D images displayed in Fig. 3 evidence that the surface of two copolymers presents nanometric aggregates. Although the frequency and size of such aggregates depend on the length of the PEG chains, the RMS roughness is very similar and noticeably low for the two materials: 11 ± 2 and

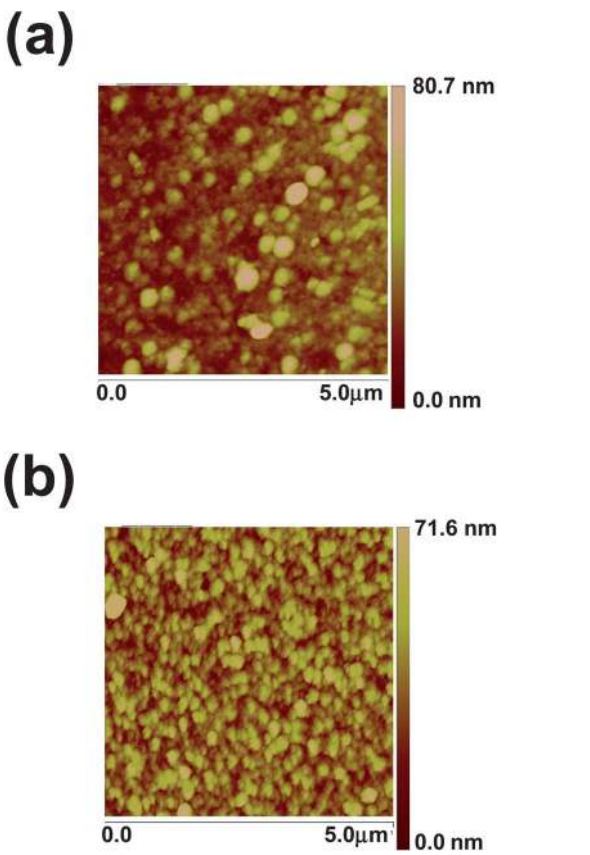

Fig. 3 2D Height AFM images of (a) PTh-*g*-PEG_{1000} and (b) PTh-*g*-PEG_{2000} prepared using $LiClO_4$ as the supporting electrolyte.

12 ± 2 nm for PTh-*g*-PEG_{1000} and PTh-*g*-PEG_{2000}, respectively. Similarly, optical profilometry measurements indicate that the films of the two grafted copolymer are ultrathin, the thicknesses being ~230 and ~110 nm for PTh-*g*-PEG_{1000} and PTh-*g*-PEG_{2000}, respectively. Accordingly, the observed $\Delta\theta = -11^\circ$ should be essentially attributed to the length of the PEG chains.

In order to compare the water-affinity of PEDOT, a polar PTh derivative that behaves as a good cellular matrix,[21,22] with that of PTh-*g*-PEG_n, ultrathin films of the former material were electrochemically prepared by CA under a constant potential of 1.40 V using acetonitrile as the generation medium and $LiClO_4$ as the supporting electrolyte. The thickness and roughness of the films obtained using a polymerization time of 10 s were ~240 nm and 111 ± 19 nm, respectively. The contact angle determined for PEDOT was $\theta = 82^\circ$ (Table 1). Considering that the roughness of PEDOT is one order of magnitude higher than those of graft copolymers, the contact angles determined for PTh-*g*-PEG_{1000} and PTh-*g*-PEG_{2000} suggest that the behavior of these graft copolymers as supportive matrices for the cell growth should be excellent (see below).

Microscopic organization of the PTh backbone and PEG chains

MD simulations in the gas-phase and aqueous solution led to very different results, as is clearly evidenced by the atomistic structures displayed in Fig. 4. Thus, inspection of snapshots selected at different time intervals indicates that, although the relative disposition of the PTh backbone and the PEG side groups is initially similar in the two environments, important differences appear after only 400 ps. More specifically, initially both PTh and PEG fragments are extended, even though the former are perpendicular to the rigid surface while the latter are parallel. This biphasic organization is preserved after 5 ns of MD in solution, the largest change being in this case the small conformational fluctuations undergone by the flexible PEG fragments. In contrast, in the gas-phase, the graft PEG chains tend to wrap the PTh backbone and the whole system collapses onto the surface. This process starts after a few hundreds of picoseconds, being completely finished after 1 ns. Thus, the desolvated environment facilitates the formation of both short- and large-range interactions, giving place to the formation of a globular structure that also interacts with the surface.

In order to provide a more quantitative view of the conformational reorganization undergone by PTh-*g*-PEG_{1000} chains in the gas-phase and solution, the temporal evolution of the end-to-end distance (d_{e-e}) for both the PTh and PEG segments is shown in Fig. 5. As it can be seen in Fig. 5a, which displays the variation of the d_{e-e} for the PTh backbone of the two explicit molecules against the simulation time, the values obtained after thermal equilibration (d_{e-e} = 70.2 and 70.8 Å) remain practically constant during the whole trajectories (averages over the whole trajectory: 67.5 ± 3.0 and 69.0 ± 3.2 Å). In contrast, the d_{e-e} drops in the gas-phase from 69.6 and 61.6 Å to ~35 Å after only 0.8 ns, which represent a drastic shrinkage of the backbone (~45% to 50%). After this, the PTh segment experiences a slight lengthening, which also takes 0.8 ns, allowing the system to alleviate the short-range repulsions generated by the fast initial contraction. Finally, the d_{e-e} values remain relatively constant at 38.8 ± 4.2 and 44.4 ± 3.5 Å during the last 3.4 ns of simulation.

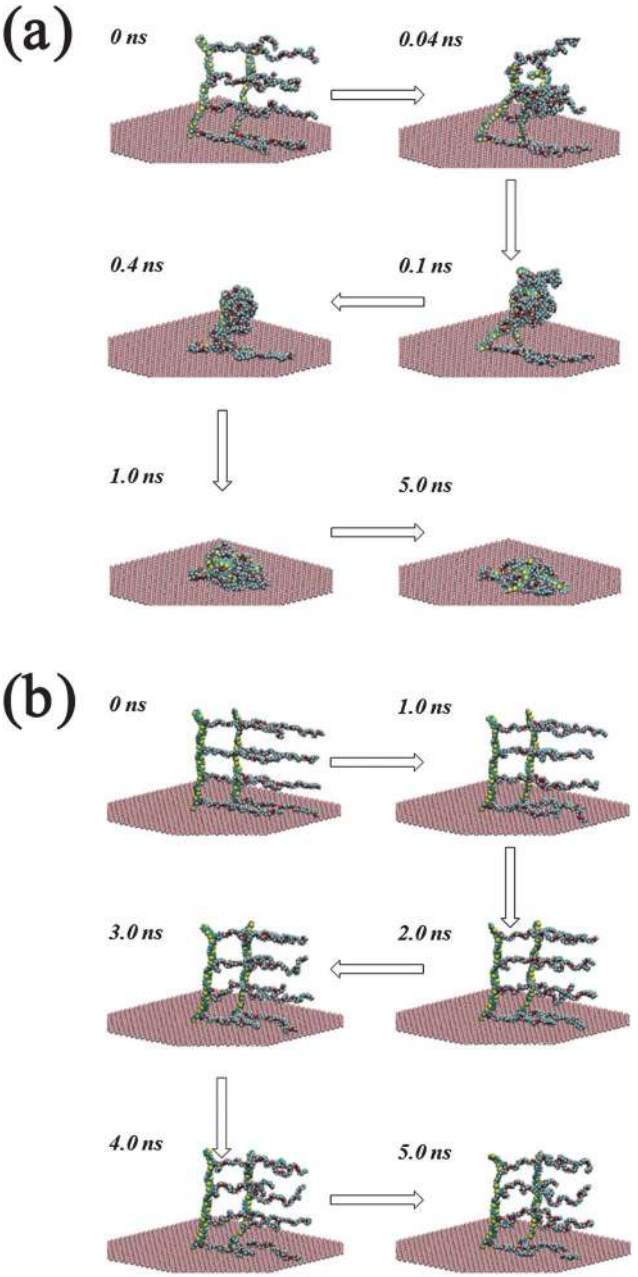

Fig. 4 Selected snapshots from MD simulations (a) in the gas-phase and (b) in solution. Water molecules and hydrogen atoms have been omitted to clarify the representations.

The three-dimensional organization of the PTh-*g*-PEG_{1000} chains has been also examined by using the partial radial distribution functions. Fig. 6a and b display the partial distributions of the S···S (g_{S-S}) and O···O (g_{O-O}) pairs, respectively, in desolvated and aqueous environments, which have been calculated considering pairs of the same molecule (*i.e.* intramolecular pairs) and the sum of both intra- and intermolecular pairs (*i.e.* all pairs). As it can be seen, comparison of

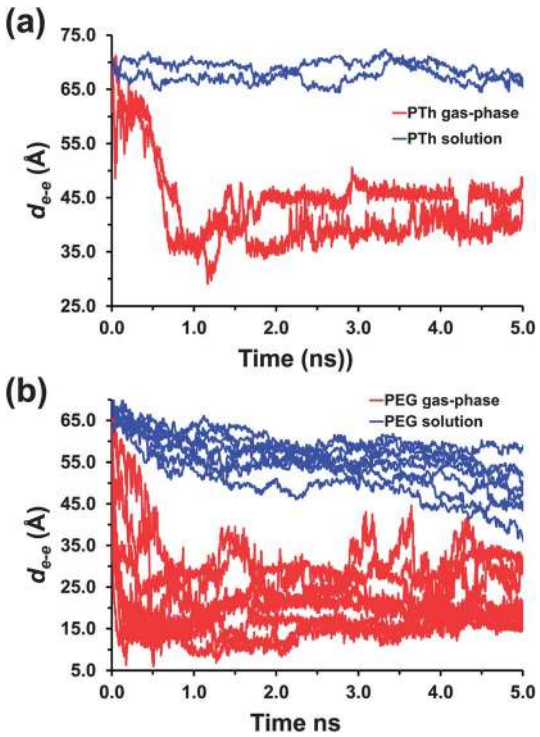

Fig. 5 Temporal evolution of the end-to-end distance (d_{e-e}) determined from MD simulations of PTh-*g*-PEG$_{1000}$ in the gas-phase (red lines) and in solution (blue lines) for: (a) PTh backbone segments (2 explicit molecules per simulation); and (b) side PEG segments (2 explicit molecules × 4 repeat units = 8 segments per simulation).

intramolecular and all pairs $g_{S-S}(r)$ and $g_{O-O}(r)$ profiles indicates that the relatively ordered organization is, as expected, dominated by the intramolecular contribution. The $g_{S-S}(r)$ shows six well-defined peaks centered at 3.45, 4.25, 7.55, 10.85, 14.25 and 18.15 Å in aqueous solution while only four peaks centered at 3.35, 4.25, 7.05 and 10.55 Å are detected in the gas-phase, the latter two being relatively undefined. This feature clearly indicates that the PTh backbone is well organized in solution, adopting a structure that is practically perpendicular to the surface, as displayed in Fig. 4b. In contrast, such a long-range order is lost in the desolvated system, the peaks at distances lower than 7.1 Å being due to the existence of short-range interactions. The $g_{O-O}(r)$ profiles show similar trends, even though the order of the PEG chains is considerably lower than that of PTh because of its intrinsic conformational flexibility, which is restricted in PTh due to the geometric restrictions of the thiophene ring. Thus, three well-defined peaks centered at 2.85, 5.55 and 8.45 Å are displayed in solution while only two peaks at 2.95 and 5.45 Å are shown in the desolvated system, the last one broad and ill-defined.

Behavior as cellular matrices

The biocompatibility of PTh-*g*-PEG$_{1000}$ and PTh-*g*-PEG$_{2000}$ doped with ClO_4^- was determined by cell adhesion and proliferation assays. The Vero cell line was selected because of its adherent growth and epithelial-like characteristics. Quantitative results of cellular adhesion assays are displayed in Fig. 7a, steel and TCPS (or culture plate) being used as control substrates. As it can be seen, the number of cells by area adhered to the surface is significantly higher for PTh-*g*-PEG$_{1000}$ and, especially, for PTh-*g*-PEG$_{2000}$ than for TCPS and steel. Thus, the hybrids do not show cytotoxic effects within a short period of time (*i.e.* 24 h), acting as excellent supportive matrices. After seven days of culture, PTh-*g*-PEG$_{2000}$ retains the same behavior while that of PTh-*g*-PEG$_{1000}$ improves considerably, indicating that this material stimulates cellular proliferation highly compared to PTh-*g*-PEG$_{2000}$ and the

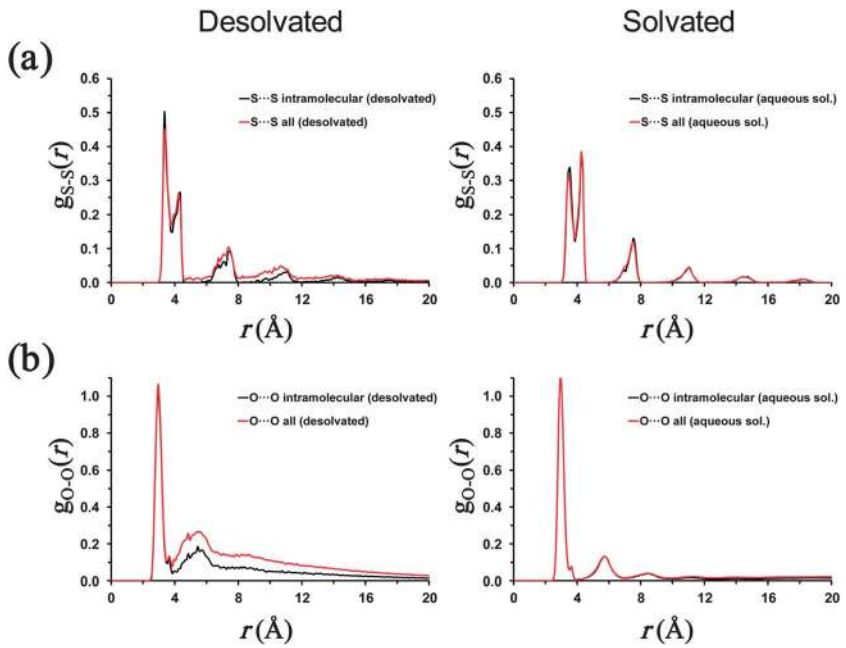

Fig. 6 Partial radial distribution functions of (a) S···S and (b) O···O pairs from MD simulations of PTh-*g*-PEG$_{1000}$ in the gas-phase (left) and in solution (right). Two profiles are displayed in each case: intramolecular pairs (black) and all pairs (red).

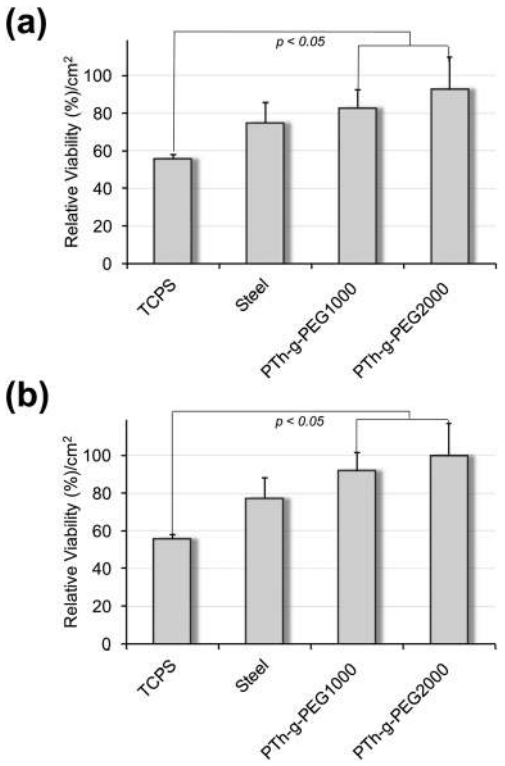

Fig. 7 Cellular adhesion (a) and cellular proliferation (b) on PTh-*g*-PEG_{1000} and PTh-*g*-PEG_{2000} doped with ClO_4^-. The relative viability of Vero cells was established in relation to the TCPS control (tissue culture polystyrene). Steel was also considered as a control substrate because the individual polymers and the blend were deposited on this material. $p < 0.05$ *vs.* TCPS.

controls. Thus, the results provided by cell proliferation assays, which are displayed in Fig. 7b, reflect that the cell viability of the two hybrids is practically the same after seven days of culture and remarkably higher than that found for poly(3,4-ethylenedioxythiophene).[38,39] The ability of PTh-*g*-PEG_{1000} and PTh-*g*-PEG_{2000} to behave as cellular matrices is clearly shown in the fluorescence images and SEM micrographs displayed in Fig. 8, which show not only the high density of adhered cells but also their homogeneous spreading onto the surface of the substrates.

Table 1 compares the response of PEDOT towards Vero cells[16] with those of PTh-*g*-PEG_{1000} and PTh-*g*-PEG_{2000}. In all cases viability is relative to the TCPS control. As it can be seen, the number of adhered cells by unit of area is similar for the three compounds, even though from a quantitative point of view it is slightly higher for PEDOT. However, the cell viability in proliferation assays is remarkably higher for the two graft copolymers than for PEDOT. This feature evidences that grafted PEG chains improve significantly the cell response of PTh and result in an excellent bioactive platform for tissue engineering.

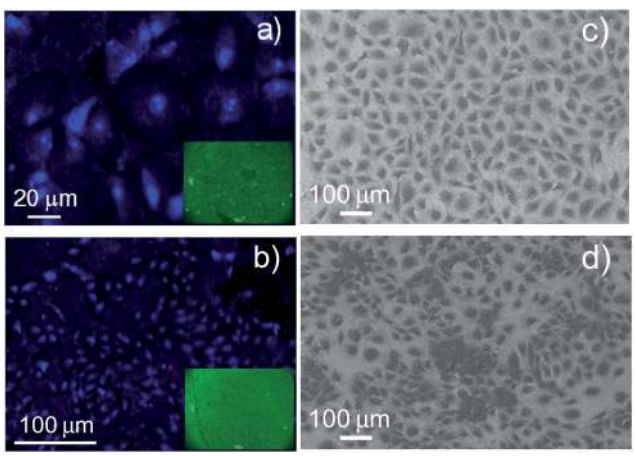

Fig. 8 Fluorescence images of cell adhesion onto (a) PTh-*g*-PEG_{1000} and (b) PTh-*g*-PEG_{2000} surfaces. Cell adhesion was observed with nuclei stain using bisbenzimide. Insets show the intrinsic fluorescence of the hybrid matrix. SEM micrographs of cells adhered onto the surface of (c) PTh-*g*-PEG_{1000} and (d) PTh-*g*-PEG_{2000}.

Electrochemical behavior of the cellular matrix

Control voltammograms of PTh-*g*-PEG_{1000} and PTh-*g*-PEG_{2000} as prepared (uncovered) and covered with Vero cells in PBS are displayed in Fig. 9a. The electroactivity of the covered films is significantly higher (*i.e.* 162 and 329%, respectively) than that of the uncovered ones, this feature being particularly remarkable for PTh-*g*-PEG_{2000}. The remarkable activity of covered films, which is higher than for PEDOT (Table 1), should be attributed to the exchange of ions promoted by the adhered cells during the oxidation–reduction process. Although the electrochemical behavior of the two hybrids is dominated by the PTh backbone, the role played by the latter effect is expected to be more important in the hybrid with smaller PEG chains, as is

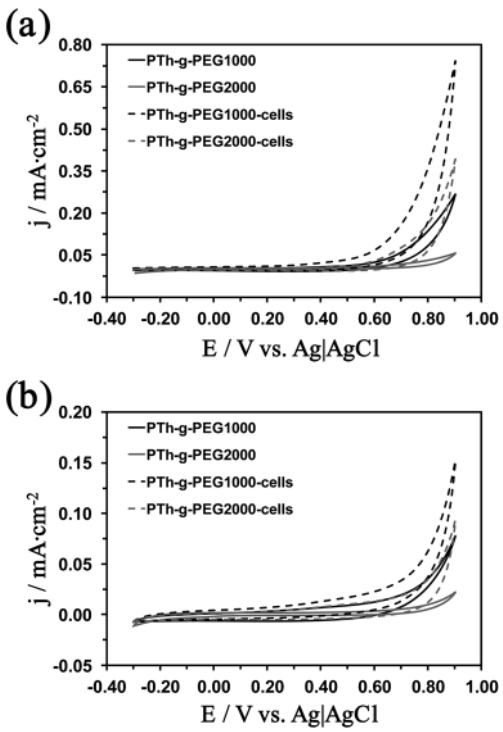

Fig. 9 Cyclic voltammograms of PTh-*g*-PEG_{1000} (black) and PTh-*g*-PEG_{2000} (grey) films uncovered (solid lines) and coated with Vero cells (dashed lines) in PBS. Voltammograms of both the as-prepared samples (a) and after ten consecutive oxidation–reduction cycles (b) are displayed.

evidenced in Fig. 9a. On the other hand, the current density at 0.90 V increases from 0.26 and 0.06 mA cm^{-2} for uncovered PTh-*g*-PEG_{1000} and PTh-*g*-PEG_{2000}, respectively, to 0.74 and 0.39 mA cm^{-2} for the systems coated with cells. This behavior also reflects the enhancement of the electrochemical properties provoked by the adhered cells.

Fig. 9b compares the voltammograms recorded after 10 consecutive oxidation–reduction cycles in PBS for samples uncovered and coated with cells. As it can be seen, there is a significant reduction in the electroactivity with respect to the control voltammograms displayed in Fig. 9a. The electrochemical stability of uncovered samples was slightly higher than that of samples coated with Vero cells. Thus, the LEA of uncovered and covered samples is ~65% and ~75%, respectively. This should be attributed to the fact that, in the first cycle, the electroactivity of the former samples in the first cycle is very low compared to that of the latter ones. Accordingly, in spite of such LEA values, the electroactivity of films coated with Vero cells is considerably higher than that of the uncoated films after 10 consecutive redox cycles (*i.e.* 79% and 228% for PBS of PTh-*g*-PEG_{1000} and PTh-*g*-PEG_{2000}, respectively).

Conclusions

UV-vis spectroscopy analyses of macromonomers indicate that the electronic properties of the pentathiophene fragment are dominated by the size of the PEG chains. This effect is significantly reduced upon polymerization and the π-conjugation of the PTh backbone plays a fundamental role in graft copolymers. The optical ε_g ranges from 2.25 to 2.29 eV, depending on the length of the PEG chain and the dopant agent. These values are ~0.3 eV larger than those typically found for 3-substituted PTh derivatives, indicating that PEG chains provoke a higher reduction in the conjugation length of the PTh backbone. Furthermore, the formation of polarons and bipolarons as well as the transition between such two states upon re-oxidation has also been detected by UV-vis spectroscopy.

The hydrophilicity of PTh-*g*-PEG_n increases with *n*, the contact angle measured for PTh-*g*-PEG_{2000} being even higher than that of PEDOT. This behavior is fully consistent with the structure predicted by MD simulations in hydrated environments. More specifically, simulations indicate that PTh and PEG segments are perpendicular and parallel to the surface, respectively, both showing extended conformations at relatively ordered arrangements. Due to this biphasic organization, polar PEG chains are completely accessible to the water molecules of the bulk. In a desolvated environment the copolymer chains collapse onto the surface, leading to an important reduction of the molecular order.

The behavior of the two hybrids as supportive matrices has been found to very good, especially that of PTh-*g*-PEG_{2000}. The two systems promote cell growth, their behavior as matrices for cellular proliferation being significantly higher than that reported for PEDOT due to the biocompatibility of the PEG fragments.[16] Furthermore, the electrochemical activity and the maximum of current density are significantly higher for PTh-*g*-PEG_n films coated with cells than for uncoated samples. The overall results suggest that the graft copolymers studied in this work have many potential biotechnological applications, especially those in which electrochemical properties are used as elements for the communication with cells (*e.g.* biosensing and transmission components in orthopedic devices).

Acknowledgements

Financial support from the MINECO and FEDER (MAT2012-34498), Generalitat de Catalunya (Research group 2009 SGR 925) is gratefully acknowledged. Support for the research of C.A. was received through the prize "ICREA Academia" for excellence in research funded by the Generalitat de Catalunya. A.D.B and I.C. acknowledge the financial support of European Social Fund – "Cristofor I. Simionescu" Postdoctoral Fellowship Programme (ID POSDRU/89/1.5/S/55216), Sectorial Operational Programme Human Resources Development 2007–2013. G.F. is thanked for the financial support through a FPI-UPC grant.

References

1 H. Shirakawa, E. J. Louis, A. G. MacDiarmid, C. K. Chiang and A. J. Heeger, *J. Chem. Soc., Chem. Commun.*, 1977, 578.
2 *Handbook of conducting polymers*, ed. T. A. Skoteheim and J. R. Reynolds, CRC Press, 3rd edn, Boca Raton, FL, 2007.
3 K. Kundu and D. Giri, *Am. Inst. Phys., Conf. Proc.*, 1996, **105**, 11075–11080.
4 S. Y. Hong and D. S. Marnick, *Macromolecules*, 1992, **25**, 4652–4657.
5 L. B. Groenendaal, F. Jonas, D. Freitag, H. Pielartzik and J. R. Reynolds, *Adv. Mater.*, 2000, **12**, 481–494.
6 S. Kirchmeyer and K. Reuter, *J. Mater. Chem.*, 2005, **15**, 2077–2088.
7 L. A. A. Pettersson, T. Johansson, F. Carlsson, H. Arwin and O. Inganas, *Synth. Met.*, 1999, **101**, 198–199.
8 A. Kumar, D. M. Welsh, M. C. Morvant, F. Piroux, K. A. Abboud and J. R. Reynolds, *Chem. Mater.*, 1998, **10**, 896–902.
9 B. Winther-Jensen, O. Winther-Jensen, M. Forsyth and D. R. MacFarlane, *Science*, 2008, **321**, 671–674.
10 J. Joo, S.-H. Park, D.-S. Seo, S.-J. Lee, H.-S. Kim, K.-W. Ryu, T.-J. Lee, S.-H. Seo and C.-L. Lee, *Adv. Funct. Mater.*, 2005, **15**, 1465–1470.
11 J. K. Koh, J. Kim, B. Kim, J. H. Kim and E. Kim, *Adv. Mater.*, 2011, **23**, 1641–1646.
12 N. K. Guimard, N. Gomez and C. E. Schmidt, *Prog. Polym. Sci.*, 2007, **32**, 876–891.
13 A. D. Bendrea, L. Cianga and I. Cianga, *J. Biomater. Appl.*, 2011, **26**, 3–84.
14 D. F. Li, H. J. Wang, J. X. Fu, W. Wang, X. S. Jia and J. Y. Wang, *J. Phys. Chem. B*, 2008, **112**, 16290–16299.
15 S. Kamalesh, P. Tan, J. Wang, T. Lee, E. T. Kang and C. H. Wang, *J. Biomed. Mater. Res.*, 2000, **52**, 467–478.
16 G. Fabregat, G. Ballano, E. Armelin, L. J. del Valle, C. Cativiela and C. Alemán, *Polym. Chem.*, 2013, **4**, 1412–1424.

17 M. M. Pérez-Madrigal, E. Armelin, L. J. del Valle, F. Estrany and C. Alemán, *Polym. Chem.*, 2012, **3**, 979–991.
18 N. Mohamed-Mahmoud and G. Olgun, *Prog. Polym. Sci.*, 2012, **37**, 1597–1656.
19 C. J. Galvin and J. Genzer, *Prog. Polym. Sci.*, 2012, **37**, 871–906.
20 V. Singh, P. Kumar and R. Sanghi, *Prog. Polym. Sci.*, 2012, **37**, 340–364.
21 D. Neugebauer, *Polymery*, 2011, **56**, 521–529.
22 C. Feng, Y. J. Li, D. Yang, J. H. Hu, X. H. Zhang and X. Y. Huang, *Chem. Soc. Rev.*, 2011, **40**, 1282–1295.
23 D. Uhrig and J. Mays, *Polym. Chem.*, 2011, **2**, 69–76.
24 P. J. Costanzo and K. K. Stokes, *Macromolecules*, 2002, **35**, 6804–6810.
25 A. Cirpan, S. Alkan, L. Toppare, Y. Hepuzer and Y. Yag, *J. Polym. Sci., Part A: Polym. Chem.*, 2002, **40**, 4131–4140.
26 J. Shen and K. Ogino, *Chem. Lett.*, 2005, **34**, 1616–1617.
27 J. Shen, K. Tsuchiya and K. Ogino, *J. Polym. Sci., Part A: Polym. Chem.*, 2008, **46**, 1003–1013.
28 X. Chen, B. Gholamskhass, X. Han, G. Vamvouinis and S. Holdcroft, *Macromol. Rapid Commun.*, 2007, **28**, 1792–1797.
29 F. Liu, Y. Chen, Y. Wei, L. Li and S. Shang, *J. Appl. Polym. Sci.*, 2012, **123**, 2582–2587.
30 A. D. Bendrea, G. Fabregat, L. Cianga, F. Estrany, L. J. del Valle, I. Cianga and C. Alemán, *Polym. Chem.*, 2013, **4**, 2709.
31 S. P. Zhong, Y. P. Zhang and C. T. Lim, *Tissue Eng., Part B: Rev.*, 2012, **18**, 77–87.
32 C. Mangold, F. Wurm and H. Frey, *Polym. Chem.*, 2012, **3**, 1714–1721.
33 J. Peyre, V. Humblot, C. Methivier, J.-M. Berjeaud and C.-M. Pradier, *J. Phys. Chem. B*, 2012, **47**, 13839–13847.
34 I. W. Hamley, M. J. Krysmann, V. Castelletto and L. Noirez, *Adv. Mater.*, 2008, **20**, 4394–4397.
35 Y. Y. Xu, J. Y. Yuan, B. Fang, M. Drechsler, M. Mullner, S. Bolisetty, M. Ballauf and A. H. E. Muller, *Adv. Funct. Mater.*, 2010, **20**, 4182–4189.
36 J. G. Sun, S. V. Graeter, L. Yu, S. F. Duan, J. P. Spatz and D. Ding, *Biomacromolecules*, 2008, **9**, 2569–2572.
37 K. Driesen, R. Van Deun, C. Gorller-Walrand and K. Binnemans, *Chem. Mater.*, 2004, **16**, 1531–1535.
38 L. J. del Valle, D. Aradilla, R. Oliver, F. Sepulcre, A. Gamez, E. Armelin, C. Alemán and F. Estrany, *Eur. Polym. J.*, 2007, **43**, 2342–2349.
39 L. J. del Valle, F. Estrany, E. Armelin, R. Oliver and C. Alemán, *Macromol. Biosci.*, 2008, **8**, 1144–1151.
40 W. D. Cornell, P. Cieplak, C. L. Bayly, I. R. Gould, K. M. Merz, D. M. Ferguson, D. C. Spellmeyer, T. Fox, J. W. Caldwell and P. A. Kollman, *J. Am. Chem. Soc.*, 1995, **117**, 5179–5197.
41 J. Wang, R. M. Wolf, J. W. Caldwell and D. A. Case, *J. Comput. Chem.*, 2004, **15**, 1157–1174.
42 J. Preat, F. Rodríguez-Ropero, J. Torras, O. Bertran, D. Zanuy and C. Alemán, *J. Comput. Chem.*, 2010, **31**, 1741–1751.
43 P. Cieplak, W. Cornell, C. I. Bayly and P. A. Kollman, *J. Comput. Chem.*, 1995, **16**, 1357–1377.
44 D. Curcó, D. Zanuy, R. Nussinov and C. Alemán, *J. Comput. Chem.*, 2011, **32**, 607–619.
45 D. Curcó, G. Revilla-López, C. Alemán and D. Zanuy, *J. Pept. Sci.*, 2011, **17**, 132–138.
46 W. L. Jorgensen, J. Chandrasekhar, J. D. Madura, R. W. Impey and M. L. Klein, *J. Chem. Phys.*, 1983, **79**, 926–935.
47 D. A. Case, T. A. Darden, T. E. Cheatham III, C. L. Simmerling, J. Wang, R. E. Duke, R. Luo, R. C. Walker, W. Zhang, K. M. Merz, B. Roberts, S. Hayik, A. Roitberg, G. Seabra, J. Swails, A. W. Goetz, I. Kolossváry, K. F. Wong, F. Paesani, J. Vanicek, R. M. Wolf, J. Liu, X. Wu, S. R. Brozell, T. Steinbrecher, H. Gohlke, Q. Cai, X. Ye, J. Wang, M.-J. Hsieh, G. Cui, D. R. Roe, D. H. Mathews, M. G. Seetin, R. Salomon-Ferrer, C. Sagui, V. Babin, T. Luchko, S. Gusarov, A. Kovalenko and P. A. Kollman, *AMBER 12*, University of California, San Francisco, 2012.
48 J. P. Ryckaert, G. Ciccotti and H. J. C. Berendsen, *J. Comput. Phys.*, 1977, **23**, 327–341.
49 L. H. Shi, F. Garnier and J. Roncali, *Macromolecules*, 1992, **25**, 6425–6429.
50 H. B. Yildiz, S. Kiralp, L. Toppare, Y. Yagci and K. Ito, *Macromol. Chem. Phys.*, 2006, **100**, 124–127.
51 F. Alakhras and R. Holze, *Synth. Met.*, 2007, **157**, 109–119.
52 A. L. Gomes, J. Casanovas, O. Bertran, J. S. de C. Campos, E. Armelin and C. Alemán, *J. Polym. Res.*, 2011, **18**, 1509–1517.
53 Y. Pang, X. Li, G. Shi and L. Jin, *Thin Solid Films*, 2008, **516**, 6512–6516.
54 J. Casanovas, D. Aradilla, J. Poater, M. Solà, F. Estrany and C. Alemán, *Phys. Chem. Chem. Phys.*, 2012, **14**, 10050–10062.
55 D. Aradilla, F. Estrany and C. Alemán, *J. Appl. Polym. Sci.*, 2011, **121**, 1982–1991.
56 G. Fabregat, C. Alemán, M. T. Casas and E. Armelin, *J. Phys. Chem. B*, 2012, **116**, 5064–5070.
57 O. Inganäs, *Chem. Soc. Rev.*, 2010, **39**, 2633–2642.
58 R. B. Pernites, R. R. Ponnapati and R. C. Advincula, *Adv. Mater.*, 2011, **23**, 3207–3213.